2-20-2021

Three-color plasmon-mediated reduction of diazonium salts over metasurfaces.

Denis A B Therien

Danielle M McRae

Claire Mangeney

Nordin Félidj

François Lagugné-Labarthet

Three-Color Plasmon-Mediated Reduction of Diazonium Salts over Metasurfaces.

Denis A.B. Therien,[1] Danielle M. McRae,[1] Claire Mangeney,[2] Nordin Félidj[3] and François Lagugné-Labarthet[1]*

[1] Department of Chemistry, University of Western Ontario, 1151 Richmond Street, London, ON, N6A 5B7, Canada.

[2] Université de Paris, Laboratoire de Chimie et Biochimie Pharmacologiques et Toxicologiques, LCBPT, UMR 8601 CNRS, F-75006 Paris, France

[3] Université de Paris, ITODYS, UMRS 7086 CNRS, F-75006 Paris, France

Abstract

Surface plasmon-mediated chemical reactions are of great interest for a variety of applications ranging from micro- and nanoscale device fabrication to chemical reactions of societal interest for hydrogen production or carbon reduction. In this work, a crosshair-like nanostructure is investigated for its ability to induce local enhancement of the local electromagnetic field at three distinct wavelengths corresponding to three plasmon resonances. The structures are irradiated

in presence of a solution containing diazonium salts at wavelengths that match the resonance positions at 532 nm, 632.8 nm, and 800 nm. The resulting grafting shows polarization and wavelength-dependent growth patterns at the nanoscale. The plasmon-mediated reactions over arrays of the crosshair structures are further investigated using scanning electron microscopy and supported by finite domain time domain modelling revealing the wavelength and polarization specific reactions. Such approach enables nanoscale molecular printing using light source opening multiplexing applications where different analytes can be grafted under distinct opto-geometric conditions.

Keywords Plasmon-mediated reaction, Metastructure, Diazonium salt, local electric field enhancement, FDTD modelling.

*Corresponding Author: flagugne@uwo.ca

Electronic Supplementary Information (ESI) available: See DOI: 10.1039/x0xx00000x

Introduction

Excitation of localized surface plasmon resonances (LSPRs) is an effective method for enhancing the local optical fields which can in turn be used for a variety of applications such as in enhanced spectroscopies and plasmonic sensing where both sensitivity and spatial resolution can be drastically improved through a plasmon effect.[1-4] In discrete nanostructures, LSPRs are generally spatially confined in specific areas and can be excited with selected set of wavelength and polarization of the impinging field. In ideal opto-geometric configuration, the electric field is typically enhanced by a 10-100 fold factor which is enough to yield large enhancement factors and which can in turn be used for a variety of sensing applications through surface enhanced mechanisms in Raman,[2, 3, 5-7] infrared,[8-10] fluorescence,[11-14] and nonlinear optical measurements.[15-18]

This spatial confinement can also be used to promote chemical reactions through the generation and ejection of hot electrons.[19] Metallic nanomaterials that contain LSPRs have shown a wide applicability for plasmon-mediated reactions.[20-22] Such reactions include chain-linking of gold nanoparticles,[23] fabrication of biosensors,[24] plasmon mediated drilling,[22] and performing surface chemistry such as CO_2 reduction,[25-27] water splitting for hydrogen production,[28-30] single oxygen production,[14] and artificial photosynthesis.[31] Multiplexed functionalization is of particular interest when several analytes can be spatially grafted over metallic structures solely using light irradiation. Such reactions have been studied on gold nanodisks by grafting both a carboxyphenyl diazonium salt and a hydroxyethyl phenyl diazonium salt to a single surface using orthogonal irradiation polarizations.[32] A polymer formulation containing two different light-emitting quantum dots was grafted to the surface of a

nanomaterial at two different polarizations, highlighting the possibility to graft quantum dots in orthogonal directions keeping at a nanoscale resolution.[33] Other plasmon-mediated reactions includes local polymerization in the vicinity of the metallic nanostructures and temperature-responsive gold/polymer hybrid structures.[34, 35] Such light-induced nanoscale printing opens many perspectives in devices fabrication. The main limitation in multi-analyte functionalization is the number of plasmon resonances that can be tackled independently with different wavelengths. A nanostructure with n discrete resonances will theoretically open the possibility to use n wavelengths of irradiations. Each resonance being associated with a unique spatial pattern of the electromagnetic confinement will subsequently yield a defined pattern upon irradiation with the matching wavelength. Such structures with multiple resonances have been demonstrated in fractal structures with resonances ranging from the visible to the mid-infrared and highlighting the hybridization between the successive fractal generations.[3, 21, 36]

In the present work, we focus on arrays of gold metastructures with crosshair geometries and that display three resonances in the visible range. The nanostructures were made by electron beam lithography and displays three resonances centered around 532, 632 and 785 nm. Specifically, we investigate the spatial grafting of 4-nitrobenzenediazonium tetrafluoroborate that have shown excellent reactivity when subject to light irradiation in the vicinity of metallic nanostructures and form a thin polymer film that can be readily observed by electron microscopy.

Materials and Methods

Finite Domain Time Domain (FDTD) modelling

The simulations throughout this study were performed using Lumerical FDTD solutions (Vancouver, Canada). The properties of the structures and substrate simulated were set using the standard Palik titanium and gold indices of refraction. [37] The structures were inscribed on a glass coverslip. The symmetric structures were inscribed using thicknesses of 3 nm for the titanium adhesion layer and 20 nm for the gold. An array of structures was set up with an average of 800 nm between individual structures in both the x- and y-directions, with periodic boundary conditions, and perfectly matched layers along the z-axis. In order to reduce the computation time, the symmetry of the structure was exploited by applying symmetry and anti-symmetry boundary conditions as appropriate. The amplitude of the input planar wave field was set to 1 V/m for the simulations, and an input light source with a wavelength range of 400 to 1000 nm was used. The near-field maps were calculated at the surface of the nanostructure at wavelengths of 530, 630, and 800 nm meanwhile the scattering spectrum was calculated in the far-field.

Electron Beam lithography (EBL)

EBL was used to prepare the crosshair nanostructures in arrays on (22×22) mm^2 glass coverslips (Thermo Fisher Scientific, ON, CA). The glass coverslips were cleaned using an O_2 plasma cleaner. Following this, poly(methyl methacrylate) in anisole (PMMA A2 950A resist, MicroChem Corp. MA, USA) was spin coated onto glass slides at 3000 rpm, corresponding to a thickness of 200 nm. Then, a conductive polymer layer (AquaSAVE, Mitsubishi Rayon America) was spin-coated over the resist to prevent loss of resolution during lithography due to charging effects. The samples

were then loaded into a scanning electron microscope (LEO 1530) and EBL was performed using the ELPHY Quantum nanolithography and nanofabrication software from Raith Nanofabrication. Following irradiation, the samples were developed in methyl isobutyl ketone:isopropanol (MIBK:IPA, 1:3 [v:v], Microchem Corp., MA, USA) for three minutes to generate the mask of the structures. Subsequently, the samples were immersed in isopropanol (VWR International LLC., ON, CA) for three minutes to stop the development process. Metal deposition was performed using an electron beam evaporation instrument (Angstrom Engineering). A 3 nm titanium adhesion layer was added at a rate of 0.8 Å/s to ensure the gold would adhere to the surface of the glass, followed by 20 nm of gold at a rate of 1 Å/s. Finally, a lift-off procedure in acetone was used to remove the mask and excess metal, leaving the desired structures and patterns as demonstrated in Fig. 2.

Diazonium salt grafting

Once the samples were prepared by electron beam lithography, they were set up on either of the two laser stages with an example shown in Scheme 1. A 5 mM solution of 4-nitrobenzenediazonium tetrafluoroborate was prepared in Milli-Q water (18.2 Ω) and drop-cast onto the surface of the substrates. A rubber O-ring was used to keep the solution on top of the array during irradiation and to prevent the samples from drying. After irradiation, the samples were washed with copious amounts of Milli-Q water and dried under a gentle flow of nitrogen gas.

Irradiation was performed using CW wavelengths at 532 nm and 632.8 nm. Irradiation at 800nm was performed with a femtosecond laser (pulse width ~200 fs, repetition rate 80 MHz). Beam size was approximately 1 µm for the 800 nm irradiation and about 8 µm for the 532 nm

and 632.8 nm lasers. The laser irradiance at the sample plane were of 1.79×10^3 W/cm^2 for 532 nm, 1.17×10^4 W/cm^2 for 632.8 nm, and 1.27×10^6 W/cm^2 for 800 nm.

Scanning Electron Microscopy (SEM)

SEM was performed using a LEO (Zeiss) 1530 field emission SEM. Since all samples were inscribed on glass coverslips, samples were coated with 5 nm of osmium prior to SEM imaging to prevent charging on the surface.

Results and Discussion

Crosshair-like nanostructures, dendrimer-like structures with C4 symmetry, were first designed and simulated using FDTD calculations, allowing their plasmon resonances to be fine-tuned prior to fabrication.

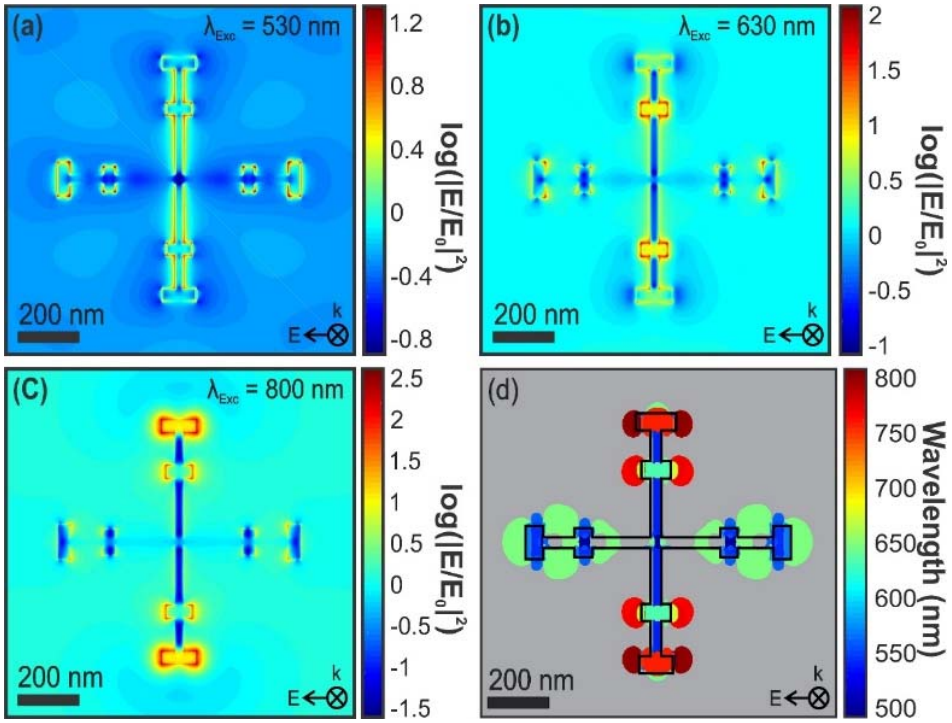

Fig. 1. Distribution of the near-field at 530 nm (a), 630 nm (b) and 800 nm (c) for a horizontal polarization. The corresponding isowavelength map is shown in (d) and represent the spatial distribution of the field for wavelengths varying from 500 nm to 800 nm with a crosshair structure outlined in black.

The near-field distribution of the EM field around the structure has been calculated at 530 nm, 630 nm and 800 nm for a horizontal polarization over the crosshair structures that are composed of orthogonal major rods with length of 800 nm and with two minor rod across each arm of the structure. Irradiation at 530 nm (Fig. 1a) shows confinement of the field along all rods, major and

minor, that are orthogonal to the polarization. At 630 nm (Fig. 1b), the two minor rods located in the middle of the branch orthogonal to the input polarization display field confinement while at 800 nm (Fig. 1c) the two minor rods located at the extremity of the branch on the arms perpendicular to the polarization direction concentrate the field the most. The isowavelength map shown in Fig. 1d provides a snapshot of the different zones where the field is locally enhanced for the three selected wavelengths. The dark blue, green and red colors indicate the field confinement at 532 nm, 632 nm and 800 nm, respectively. The structure being isotropic with a C_4 symmetry axis, a rotation of the polarization by 90° will rotate the distribution pattern accordingly.

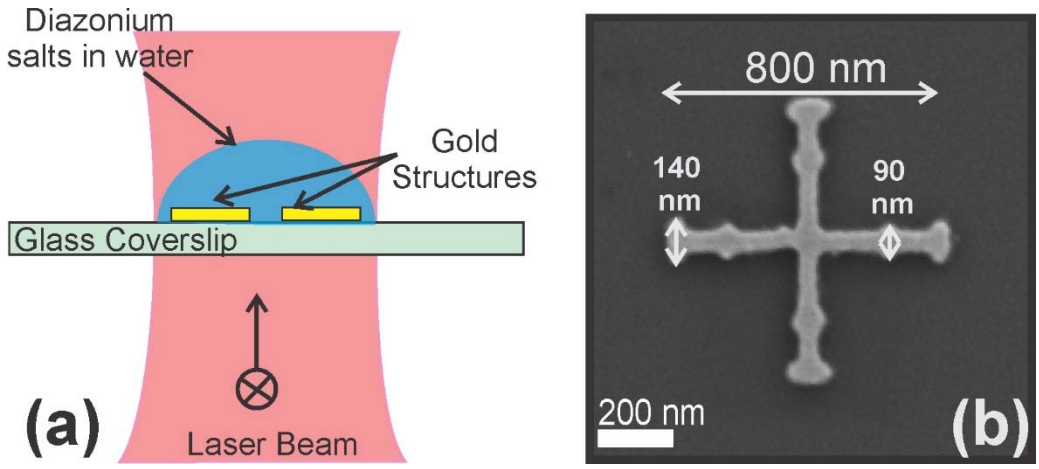

Fig. 2. (a) Depiction of a grafting experiment. (b) Produced individual structures.

Two distinct optical setups were used to investigate the three LSPRs. An 800 nm femtosecond-pulsed laser is used to irradiate a single structure at a time without burning or destroying them. This setup also uses a piezoelectric nanopositioning stage combined with a 100× objective (N.A.=0.95). This combination allows the 1 µm laser spot to be precisely positioned onto a single structure at a time. The CW lasers at 532 nm and 632.8 nm were coupled to a distinct setup that

uses a 20x objective (N.A.=0.5) that is slightly defocused producing a spot size of approximately 8 µm and irradiating multiple structures at the same time. While this setup has the advantage of irradiating many structures at once, the Gaussian nature of the beam produces varying results from the center of the spot towards the edge, which will be discussed further. A typical irradiation experiment is shown in **Fig. 2a** together with a single nanostructure produced by electron-beam lithography **(Fig. 2b).**

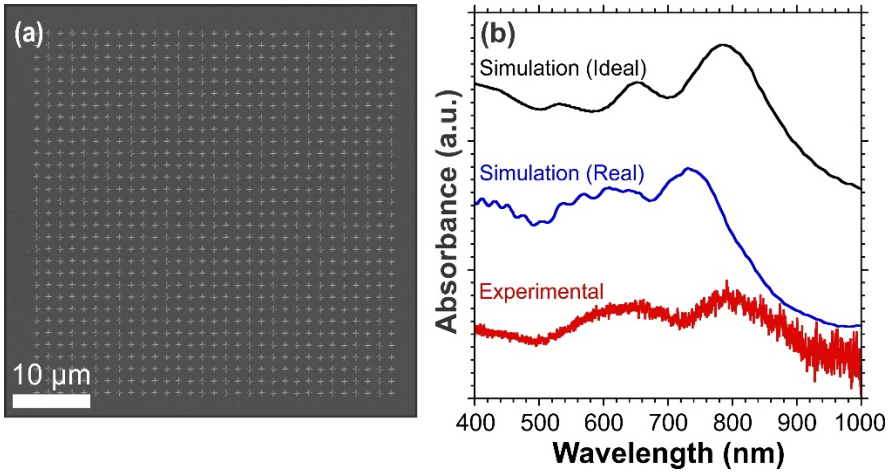

Fig. 3. (a) Representative SEM image of an array of dendrimers used for grafting with a single structure shown in the inset. **(b)** FDTD far-field scattering for ideal (defect-free) and real structures (as shown in Fig. 1b) and experimental absorption measurements for a linearly polarized light oriented horizontally or vertically with respect to the structure axes.

Using electron beam lithography, arrays of structures were produced in (50×50) μm^2 patches, as shown in Fig. 3a. The individual crosshairs major axes measure 800 nm in length with 90 nm and 140 nm minor notches oriented perpendicularly to the longer branches (Fig. 2b). Three broad plasmon resonances can be identified in the far-field FDTD modelling at central wavelengths of

530 nm, 630 nm, and 800 nm (Fig. 3b). The experimental extinction spectrum only shows 2 resonances including a broader one centered at 610 nm that shows a shoulder around 550 nm.

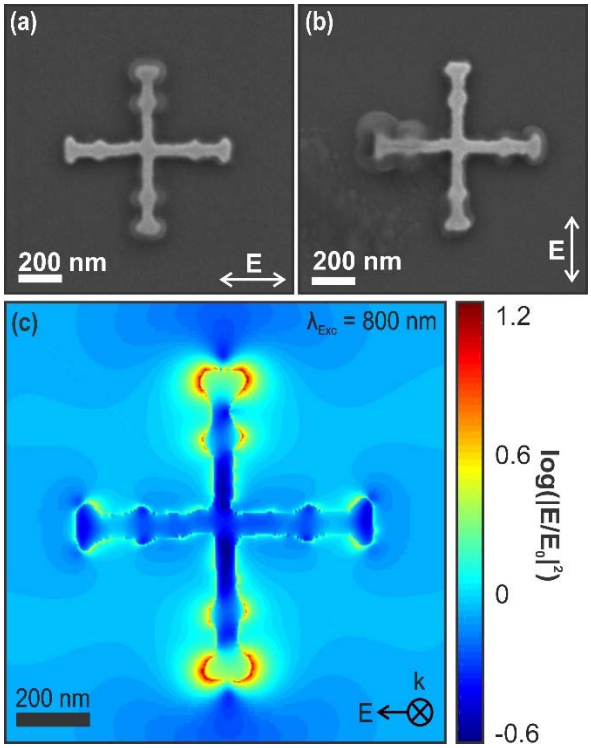

Fig. 4. SEM images of the dendrimers after irradiation under an 800 nm fs-pulsed laser, for both **(a)** horizontally and **(b)** vertically polarized light. **(c)** FDTD modelling of the near-field distribution upon irradiation at 800 nm for the real structure with a horizontal polarization.

The crosshair structures were first irradiated at 800 nm for 60 seconds under a power of 10 mW. The material grafted is composed of a thin film formed from 4-nitrobenzenediazonium tetrafluoroborate,[38] through either a cationic or a radical plasmon-induced polymerization pathway.[39] Briefly, in the cationic process, heating in room temperature conditions or light-induced decomposition of the solution-containing salt induces the formation of cations by heterolytic dediazoniation that react with gold surfaces. Other aryl cations present in solution

further react with the first grafted groups forming polyaryl layer on the surface.[40] This cation-induced reaction is generally referred as a spontaneous grafting and may lead to the formation of monolayer at the surface of the substrate.[39, 41] In the radical process, plasmon-induced electron transfers from the gold structures to the diazonium cation yield the formation of aryl radicals that in turn react with the surface to form an aryl molecular layer. Other radicals react with the first layer to form a thin polymer film which thickness varies with the irradiation conditions and local field enhancements. Both mechanisms presumably yield the formation of polymer thin films in the area where the field is maximum. However, local heating effect from a cationic process will dissipate very quickly in the solution and because of the good thermal conductivity of the gold structures, the grafting will be more homogeneous over the surface of the structure. Additionally, the light decomposition of the salts occurs predominantly in the ultra-violet range and should be limited upon exposure at 800 nm. The grafting at 800 nm should essentially be driven by a radical mechanism. Shown in Figs. 4a,b are the SEM images after irradiation at λ=800 nm with a horizontal and vertical polarization, respectively. The polarization dependence is the most apparent here, where the orthogonal irradiations produced similar grafting patterns rotated by 90°. These experimental results can be compared to the FDTD calculations shown in Fig. 1c and Fig. 4c for ideal and real structures, respectively. The plasmon-induced grafting of the diazonium salts is predominantly localized around the two minor notches on the perpendicular branch with respect to the input polarization. While the irradiance is higher on the 800 nm setup (by a factor of 100 – 1000), the femtosecond pulses allow the structures to be irradiated without burning or melting them. The same localized molecular patterning can be

done over an array of structures irradiated in similar conditions, as shown in Fig. S1, highlighting the reproducibility and homogeneity of the plasmon-induced reaction.

Furthermore, as shown in the inset of Fig. S1 with a reference structure immersed with the same solution but without any laser irradiation, this experiment indicates that there is no evidence of spontaneous grafting at the surface of the crosshairs and that the grafting is only plasmon-driven, as expected.

Similar structures were irradiated with a continuous-wave laser at 632.8 nm with a spot size of approximately 8 μm in diameter. A manual control stage was used, allowing for the irradiation of multiple structures at a time. This led to some variety in the grafting development based on the energy dose that each structure received relative to its position in the laser spot.

Shown in Figs. 5a,b are the polarization dependent grafting spatial distributions for both horizontally (Fig. 5a) and vertically (Fig. 5b) polarized fields. The grafted material has been colorized for the corresponding polarizations in Fig. 5c,d. Remarkably, the grafting occurs on both axes. However, the major axis orthogonal to the input polarization show the thicker grafting. This is again in agreement with the FDTD calculation of Fig. 1b for the ideal and real structures and Fig. 5e for the real structure where both major axes show areas of large confinement yet with larger confinement on the axes orthogonal to the input polarization. In order to estimate the effect of the irradiation power over the grafting, functionalized areas were imaged at the center of the beam and in the outer edge of the Gaussian beam.

At the center of the 632.8 nm beam (Fig. S2a,b and Fig. S3a,b) the grafting is homogeneous over the whole structure and it is difficult to differentiate the areas with different field enhancements. In contrast, Fig. S2a,c and Fig.S3a,c corresponds to the area at the edge of the

632.8 nm Gaussian beam, the functionalization is partial and shows grafting along the orthogonal axis up to the first notch and around the larger notch of the axis parallel to the input polarization, in good agreement with Fig. 1b. This indicates that the threshold for plasmon-mediated grafting is relatively low. By fine tuning the energy density at the surface, the amount of material grafted can be controlled. This can be achieved by either reducing the irradiation time or the irradiance.

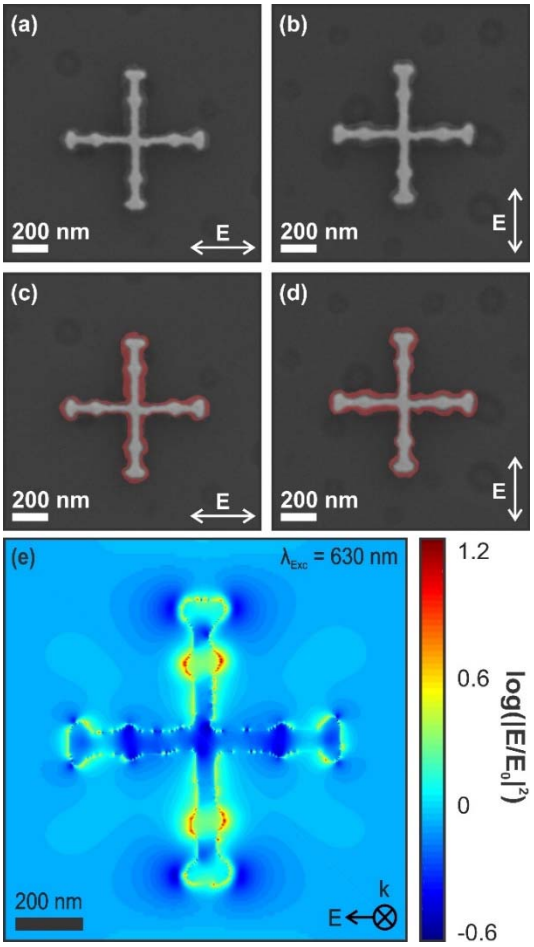

Fig. 5. SEM images of the structures after irradiation under a 632.8 nm continuous-wave laser, for both **(a)** horizontally and **(b)** vertically polarized light. **(c,d)** represents the same images but colorized in red to highlight the areas on which grafting mainly occurred. **(e)** FDTD modelling of the near-field distribution upon irradiation at 630 nm for the real structure with a horizontal polarization.

Finally, the last experiment was done with an irradiation at 532 nm, a wavelength for which FDTD predicts a third but weaker resonance. The extinction spectra (Fig. 2b) show that the resonance appears to be superimposed with a broader resonance centered at 630 nm.

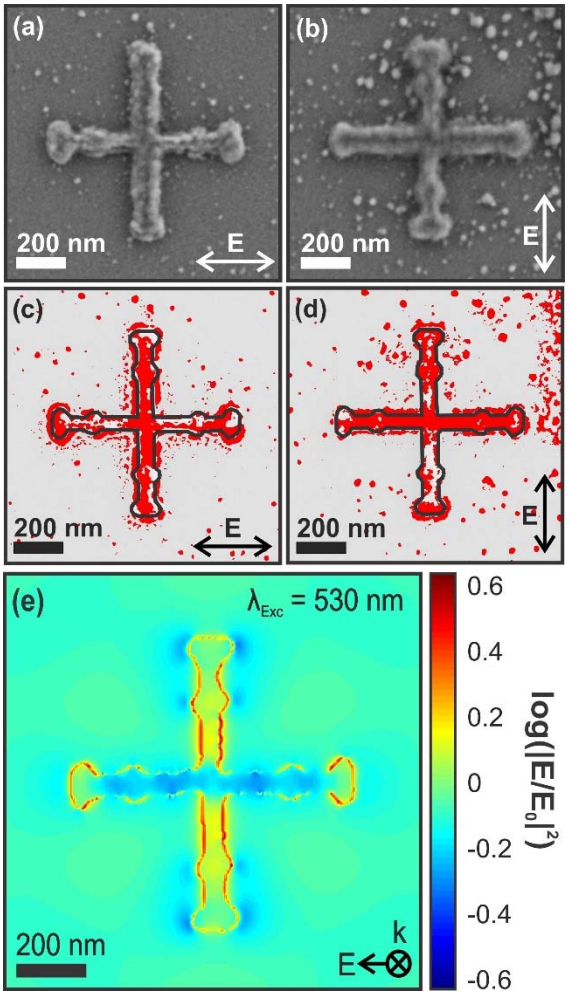

Fig. 6. SEM images of the crosshairs after irradiation under a 532 nm laser both **(a)** horizontally and **(b)** vertically polarized. **(c)** and **(d)** are the colorized images of **(a)** and **(b)**, respectively, with the outline of the cross in black as a guide for the eye. **(e)** FDTD modelling of the near-field distribution upon irradiation at 530 nm for the real structure with a horizontal polarization. Reference background image used to generate (c) and (d) is provided in Fig. S4.

Shown in Fig. 6a,b are the SEM images of individual nanostructures after irradiation in the presence of the diazonium solution with a horizontal and a vertical polarization, respectively. Figs 6c,d are treated images obtained by subtracting the bare non-functionalized structure (Fig S4) and that shows the spatial distribution of the polyaryl films. Both major arms appear to experience grafting yet with predominant grafting along the major arms that are orthogonal to the input polarization. In both case the gold structure is entirely covered by the polyaryl layers derived from the diazonium salt which appear thicker than when irradiated at 800 or 632.8 nm. Interestingly, the irradiation at 532 nm appears to induce polymerization on the substrate as well, as shown by the numerous aggregates located around the structures. The presence of such aggregates is not observed in any of the experiments performed at 632 nm and 800 nm. Presumably the presence of these aggregates over the gold structure and the glass surface is facilitated by spontaneous grafting enabled by the higher energy 532 nm photons that would yield more thermally induced decomposition and subsequent grafting through the cationic process.

The LSPR present at 532 nm originates from the width of the structures themselves (Fig. 1a and Fig. 6e), which is perpendicular to the irradiation polarization. This can be seen by the growth occurring on all the outer features, and predominantly on the entire arm, perpendicular to the irradiation polarization as highlighted in red in Fig. 6a-d where the notches cannot be distinguished anymore since they are completely covered by the polyaryl layer.

The polarization dependent grafting demonstrates the effectiveness of the nanostructure's response upon irradiation. Shown in Fig. S5, are a series of crosshair structures located at the

edge of the irradiation beam polarized vertically (Fig. S5a) and horizontally (Fig. S5b) with intensity increasing from left to right.

The bare structures on the left-most of Fig. S5a,b are out of the beam while it transitions to irradiation with the highest power on the right. These experiments show again that the major axes oriented perpendicular to the polarization of the impinging beam experience the most functionalization where the grafted molecules completely cover the major axis masking even the two smaller orthogonal notches.

The progression of the grafting across the surface indicates that the density of hot electrons generated upon irradiation at 532 nm are proportional to the energy dose. It can also be seen in these images that the structures on the left have no molecules adhered to either the surface of the structures, or the glass substrate itself. On the right, however, there is a large grafting visible on the structures as well as organic aggregates adsorbed on the surface. This demonstrates that all the grafting is occurring due to the irradiation, and not spontaneously. While the 532 nm grafting had the lowest irradiance of the three tests at 1.79×10^3 W/cm^2, the grafting was more prominent for equivalent irradiation times (60s). This is caused by the LSPR, which covers a larger surface area of the crosshair structure than the other two resonances, in synergy with the cationic process as evidenced by the numerous organic deposits observed at the surface of the glass coverslip closer to the center of the laser spot.

In summary, the different grafting patterns based on the irradiation wavelength are shown. The electromagnetic enhancement hotspots from the plasmon resonances play an important role when comparing these different grafting patterns. By changing the irradiation source as well as the polarization, molecules were grafted to specific areas of the surface. Although this work

considers only a selected diazonium salt, there is potential to use these structures to graft up to six different molecules onto the same surface using three wavelengths and two polarization states. This versatility can be taken advantage of for molecular patterning. This opens new applications in molecular electronics and biosensing where distinct grafted molecules within a nanoscale structure can display different functions.

Conclusion

Crosshair nanostructures with three plasmon resonances were designed and fabricated in order to facilitate plasmon-mediated reactions in the visible wavelength region. The structures were successfully employed for the surface specific grafting of a diazonium salt to the surface using wavelengths of 532 nm, 633 nm, and 800 nm. For each of the wavelengths, distinct grafting patterns can be observed around the structures. The polarization dependence of the grafting was also tested for these three wavelengths to which the structures responded according to the incident polarization. These nanostructures offer a platform for a multitude of applications in both chemistry and nanoscale surface patterning due to the possibility to spatially control the functionalization of distinct molecules with a selected set of wavelength and polarization. Based on this approach, optical sensing devices with multiplexed specificity or bioconjugation could be developed.

Author contributions

D.A.B.T. has made the structures, collected the spectra, and performed the grafting experiments and SEM imaging. D.M.M. has performed the FDTD calculations. C.M., N.F. and F.L.L have directed the work conceptually and experimentally. All authors have participated to the writing of the manuscript.

Conflicts of Interest

There are no conflicts to declare.

Acknowledgements

The authors would like to gratefully acknowledge the Nanofabrication Facility at the University of Western Ontario for their assistance in fabricating the crosshair arrays. The authors would also like to thank the Natural Sciences and Engineering Research Council (NSERC) for funding this project through grant (RGPIN2020-06676).

References

1. T. T. X. Ong, E. W. Blanch and O. A. H. Jones, *Sci. Total. Environ.*, 2020, **720**, 137601.
2. D. Kurouski, A. Dazzi, R. Zenobi and A. Centrone, *Chem. Soc. Rev.*, 2020, **49**, 3315-3347.
3. G. Q. Wallace and F. Lagugné-Labarthet, *Analyst*, 2019, **144**, 13-30.
4. F. Zen, V. D. Karanikolas, J. A. Behan, J. Andersson, et al., *Langmuir*, 2017, **33**, 4198-4206.
5. J. Zhou, T. Yang, J. Chen, C. Wang, et al., *Coord. Chem. Rev.*, 2020, **410**, 213218.
6. H. Zhang, S. Duan, P. M. Radjenovic, Z.-Q. Tian, et al., *Acc. Chem. Res.*, 2020, **53**, 729-739.

7. M. Sharifi, S. H. Hosseinali, R. Hossein Alizadeh, A. Hasan, et al., *Talanta*, 2020, **212**, 120782.
8. G. Q. Wallace, S. T. Read, D. M. McRae, S. M. Rosendahl, et al., *Adv. Opt. Mater.*, 2018, **6**, 1701336.
9. G. Q. Wallace, H. C. Foy, S. M. Rosendahl and F. Lagugné-Labarthet, *J. Phys. Chem. C*, 2017, **121**, 9497-9507.
10. N. Bareza, Jr., K. K. Gopalan, R. Alani, B. Paulillo, et al., *ACS Photonics*, 2020, **7**, 879-884.
11. J.-F. Li, C.-Y. Li and R. F. Aroca, *Chem. Soc. Rev.*, 2017, **46**, 3962-3979.
12. M. Bauch, K. Toma, M. Toma, Q. Zhang, et al., *Plasmonics*, 2014, **9**, 781-799.
13. T. Ming, L. Zhao, Z. Yang, H. Chen, et al., *Nano Lett.*, 2009, **9**, 3896-3903.
14. M. Tavakkoli Yaraki, S. Daqiqeh Rezaei and Y. N. Tan, *Phys. Chem. Chem. Phys.*, 2020, **22**, 5673-5687.
15. D. A. B. Therien, R. Hou and F. Lagugné-Labarthet, *Plasmonics*, 2020, **15**, 507-515.
16. D. M. McRae, D. A. B. Therien, R. Hou, G. Q. Wallace, et al., *ACS Appl. Nano. Mater.*, 2020, **3**, 3922-3929.
17. X. Lin, Y. Liu, K. Wang, C. Wei, et al., *ACS Nano*, 2018, **12**, 689-696.
18. J. Butet, P.-F. Brevet and O. J. F. Martin, *ACS Nano*, 2015, **9**, 10545-10562.
19. S. Yu and P. K. Jain, *Angew. Chem. Int. Edit.*, 2020, **59**, 2085-2088.
20. M. Ha, J.-H. Kim, M. You, Q. Li, et al., *Chem. Rev.*, 2019, **119**, 12208-12278.
21. I. C. Bicket, E. P. Bellido, D. M. McRae, F. Lagugné-Labarthet, et al., *ACS Photonics*, 2019, **6**, 2974-2984.
22. D. M. McRae, K. Jeon and F. Lagugné-Labarthet, *ACS Omega*, 2018, **3**, 7269-7277.
23. S. Pal, A. Dutta, M. Paul and A. Chattopadhyay, *J. Phys. Chem. C*, 2020, **124**, 3204-3210.
24. D. Hetemi, V. Noel and J. Pinson, *Biosensors*, 2020, **10**, 4.
25. S. Wallentine, S. Bandaranayake, S. Biswas and L. R. Baker, *J. Phys. Chem. A*, 2020.
26. C. Lu, J. Li, J. Yan, B. Li, et al., *Appl. Mater. Today.*, 2020, **20**, 100744.
27. S. Yu and P. K. Jain, *Nature Commun.*, 2019, **10**, 2022.
28. Y. Sang, B. Liu, T. Tao, D. Jiang, et al., *Semicond. Sci. Tech.*, 2020, **35**, 025017.
29. Y.-S. Huang, Y.-C. Hsiao, S.-H. Tzeng, Y.-H. Wu, et al., *Nano Energy*, 2020, **77**, 105267.

30. D. Ghosh, K. Roy, K. Sarkar, P. Devi, et al., *ACS Appl. Mater. Inter.*, 2020, **12**, 28792-28800.
31. D. Kumar, C. H. Park and C. S. Kim, *J. Mater. Chem. A*, 2020, **8**, 5734-5743.
32. I. Tijunelyte, I. Kherbouche, S. Gam-Derouich, M. Nguyen, et al., *Nanoscale Horiz.*, 2018, **3**, 53-57.
33. X. Zhou, J. Wenger, F. N. Viscomi, L. Le Cunff, et al., *Nano Lett.*, 2015, **15**, 7458-7466.
34. H. Gehan, L. Fillaud, M. M. Chehimi, J. Aubard, et al., *ACS Nano*, 2010, **4**, 6491-6500.
35. Y. Wang, S. Wang, S. Zhang, O. A. Scherman, et al., *Nano Research*, 2018, **11**, 6384-6390.
36. D. M. McRae and F. Lagugné-Labarthet, *Nat. Nanotechnol.*, 2019, **14**, 922-923.
37. E. Palik, *Handbook of Optical constants of Solids*, Academic Press, Burlington, 1997.
38. J. Pinson and F. Podvorica, *Chem. Soc. Rev.*, 2005, **34**, 429-439.
39. A. Mesnage, X. Lefèvre, P. Jégou, G. Deniau, et al., *Langmuir*, 2012, **28**, 11767-11778.
40. M. Nguyen, A. Lamouri, C. Salameh, G. Levi, et al., *Nanoscale*, 2016, **8**, 8633-8640.
41. D. R. Jayasundara, R. J. Cullen, L. Soldi and P. E. Colavita, *Langmuir*, 2011, **27**, 13029-13036.